energies

MDPI

Article

Shielding Design Optimization of the Helium-Cooled Pebble Bed Breeding Blanket for the EU DEMO Fusion Reactor

Iole Palermo [1,*], Francisco A. Hernández [2], Pavel Pereslavtsev [2], David Rapisarda [1] and Guangming Zhou [2]

[1] CIEMAT, Fusion Technology Division, Avda. Complutense 40, 28040 Madrid, Spain
[2] Karlsruhe Institute of Technology (KIT), 76131 Eggenstein-Leopoldshafen, Germany
* Correspondence: iole.palermo@ciemat.es

Abstract: The helium-cooled pebble bed (HCPB) breeding blanket (BB) is one of the two driver-blanket candidates for the European DEMO fusion reactor. Recent design activities were focused, among other objectives, on the achievement of an efficient shielding system to adequately protect the vacuum vessel (VV) and toroidal field coils (TFCs). Several shielding options have been studied in terms of architecture (e.g., in-BB shield and ex-BB shield) and materials (e.g., B_4C, WC, WB, YHx, and ZrHx). In this study, the B_4C material was selected as the most attractive option considering not only shielding performance but also availability, industrialization, experience, and cost factors. Subsequently, we performed a parametric study by implementing different thicknesses of a B_4C external shield and reporting information of its effect on shielding performance, structural behavior, swelling and tritium breeding. Furthermore, a detailed structure for the VV was developed considering an internal layered configuration comprising steels/water with different boron contents. Corresponding shielding analyses were conducted regarding influence on neutron attenuation when implementing such a VV structure for both the baseline consolidated design of the HCPB and one of the previously developed and improved BSS configurations. The most critical responses (neutron flux and dpa) were fully established only using 10 cm B_4C and an improved VV configuration.

Keywords: shielding; boron carbide; HCPB blanket; DEMO; neutronics; nuclear fusion

Citation: Palermo, I.; Hernández, F.A.; Pereslavtsev, P.; Rapisarda, D.; Zhou, G. Shielding Design Optimization of the Helium-Cooled Pebble Bed Breeding Blanket for the EU DEMO Fusion Reactor. *Energies* **2022**, *15*, 5734. https://doi.org/10.3390/en15155734

Academic Editor: Hiroshi Sekimoto

Received: 14 July 2022
Accepted: 28 July 2022
Published: 7 August 2022

1. Introduction

The helium-cooled pebble bed (HCPB) breeding blanket (BB) is one of the two driver-blanket candidates for the European DEMO fusion reactor.

Recent design activities [1] were focused, among other objectives, on the achievement of an efficient shielding system to protect adequately the vacuum vessel (VV) and toroidal field coils (TFCs).

During the pre-concept design (PCD) phase of the European DEMO program (from 2014 to 2020), several shielding options were studied in terms of architecture (e.g., in-BB shield and ex-BB shield) and materials (e.g., B_4C, WC, WB, YHx, and ZrHx). Some of the results are summarized in [1–3].

The most attractive designs have been those based on an external arrangement of WC, $YH_{1.6}$ or B_4C blocks that are passively cooled by thermal radiation towards the BB backplate and the VV. Additional configurations and analyses have been performed for these designs, as described in Section 3.

Based on such studies, an enhanced HCPB configuration was developed in 2021, when the European DEMO program entered the concept design (CD) phase (2021–2027). For this configuration, a parametric study was performed (Section 4) in which we implemented different thicknesses of a B_4C external shield located in the back-supporting structure (BSS) behind the breeder zone (BZ) or behind the Eurofer BSS and reporting information of its effect on shielding performance (in terms of nuclear heating, neutron flux and displacement per atom (dpa) in the TFCs), structural behavior (nuclear heating, helium production and

dpa inside the VV), swelling (helium production inside the B_4C), and tritium breeding (tritium breeding ratio (TBR) and local tritium production inside the breeder and B_4C).

Furthermore, a detailed structure for the VV was developed (Section 5) considering an internal layered configuration comprising steels/water with different boron contents. Corresponding shielding analyses were conducted regarding influence on neutron attenuation when implementing such a VV structure for both the baseline consolidated design of the HCPB and one of the previously developed and improved BSS configurations.

Methodology for Neutronic Studies

Neutronic studies have entailed the use of the Monte Carlo code MCNP5v1.6 [4] and the nuclear cross-sections from JEFF3.2 nuclear data libraries [5] for transport simulations and the use of SuperMC [6] for modeling and CAD/MCNP conversions.

The Joint Evaluated Fusion File JEFF3-2 and the latest version JEFF 3-3 comprise the reference nuclear data library for EUROfusion. Processed ACE data libraries for use with MCNP are provided by the NEA Data Bank of the OECD, Paris. The data files can be downloaded from the NEA web site at [5] without any access restriction.

The radial profiles for the different neutronic responses were extracted from mesh tally 3D maps.

The FMESH card used in MCNP [4] allows the user to define a mesh tally superimposed over the problem geometry. By default, the mesh tally calculates the track length estimate of the particle flux averaged over a mesh cell in units of particles/cm^2. When used in combination with different tally multiplier (FM) cards that include the material (and thus the cross-section information) and the MT reaction number, it is possible to compute not only the fluxes but also (as in our case) the nuclear heating, the T and helium production, and the displacement per atom (dpa). The dpa calculation follows the standard NRT model [7], calculating the number of atomic displacements produced in a damage cascade via a primary knock-on atom of known energy.

Different resolutions were used in the mesh tallies for the different zones: high resolution for the space occupied by the BB and BSS and medium resolution for the VV and TFC. In general, detailed radial profiles were obtained from mesh tallies with:

- One bin of 50 cm for Z (at Z = 0–50 cm), i.e., at the equatorial most irradiated zone.
- One bin of 5 cm in Y direction.
- Radial bins in X direction of:
  - One centimeter from X = 581 cm to X = 500 cm (a radial zone corresponding to the BB and BSS zone plus the first 3 cm of the VV).
  - Five centimeters from 500 cm to 360 cm of depth (corresponding to the rest of the VV and the TFC).

Furthermore, to achieve results with accurate statistics inside the TFC, we employed a variance reduction technique to improve importances (IMPs) from the VV to the TFC. Therefore, we were able to obtain results with strong statistics thanks to IMP settings and 10^9 particles launched. The values of relative uncertainties were less than 0.05 (5%) up to coordinate x = 402.5 cm, which was deep inside the TFC WP.

2. The HCPB BB Design for the EU DEMO

The current HCPB reference design was developed on the so-called DEMO1 tokamak Baseline2017. The main parameters of this baseline are R0 = 9.0 m, A = 3.1, tburn = 2 h, tdwell = 600 s, Pfus = 1998 MW, 16 toroidal field coils (TFCs), and an outboard (OB) blanket thickness of about 1 m [8–10].

The current HCPB is based on a single-module segment (SMS) architecture instead of the previous multi-module segment (MMS) one. The SMS blanket housing is formed by a 20 mm thick, U-shaped-like first wall (FW) with a 30 mm back plate and a so-called back-supporting structure (BSS) containing the segment's coolant manifolds [11]; see Figure 1. The plasma-facing side of the FW is coated with a 2 mm thick W armor, and it is expected to have a roof-top shape with a gradient of ~2°.

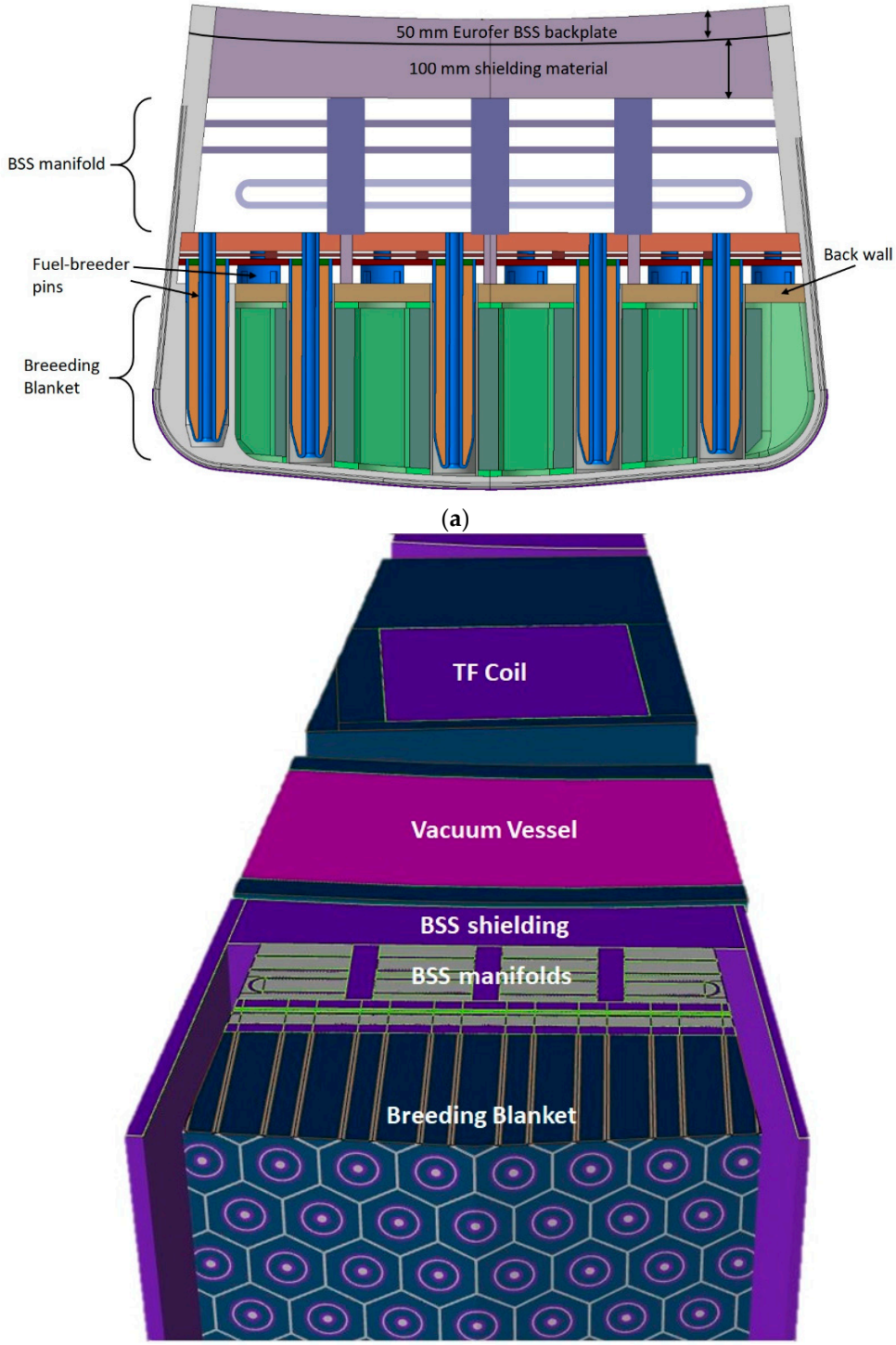

Figure 1. HCPB BB CAD model and proposed BSS segmentation for shielding assessments (**a**); neutronic detailed model of the BB, BSS, VV and TFC (**b**).

Several design iterations were required during the PCD phase in order to adjust the design to the current demanding DEMO requirements, to the challenging system integration, and to the need to keep near-term technologies. In this respect, the design evolved to a so-called fuel-breeder pin architecture built in single-module segments [1]. Each pin contains co-axial tubes that form annular cells for inlet and outlet He channels, as well as for the placement of a tritium breeder ceramic; see Figure 1. The current HCPB

DEMO design [1] implies the use of mixed Li_4SiO_4 plus 35 mol.% of Li_2TiO_3 with 60% ^6Li enrichment ceramic breeder material in the form of pebble beds inside the pins. The space around the pins is filled with $Be_{12}Ti$ hexagonal prismatic blocks that serve as neutron multipliers that are separated by 10 mm gaps, which allows for their thermal expansion and the flow of the purge gas. This purge gas (He + 0.1%vol. H_2 at 0.2 MPa) flows through the ceramic breeder, extracting tritium from functional materials, and transporting it towards the Tritium Extraction and Removal system. He at 8 MPa is used as the coolant, with a temperature window of 300–520 °C. The pitch between pins (130 mm in the IB and 125 mm in the OB sides) was optimized to provide the maximum TBR, minimize the number of pins, and ensure the reliable cooling of the blanket structure.

Li_4SiO_4 has a higher Li atomic density, so it is superior to Li_2TiO_3 in terms of T breeding. However, Li_2TiO_3 has a significantly higher crush load strength than Li_4SiO_4. This has been a main motivator in the search for a modified Li_4SiO_4 breeder material with the addition of Li_2TiO_3 [12] in order to improve the mechanical properties of the resulting compound [13–15], leading to the so-called advanced ceramic breeder material that is currently being developed for the EU DEMO HCPB.

This architecture has proven to achieve strong tritium breeding performance (TBR≈1.18 with 60% enrichment of ^6Li and TBR ≈ 1.20 with 70% enrichment of ^6Li) and a remarkably low plant circulating power (<100 MW), and its design for manufacturing paves the way for a better industrialization and improved reliability. The main issues of this promising configuration are related with the shielding of the VV and the TFCs, to which the studies reported in this paper are dedicated.

3. Material Selection for BSS Shielding

Several materials, including metal hydrides, tungsten compounds, boron carbide and pressurized water, were proposed in previous works [3,16] for shielding purposes. Two options for the shield arrangement in the HCPB blanket were verified: inside and outside the back-supporting structure (BSS) of the blanket. The most effective options in terms of dpa accumulation in the inner wall of the vacuum vessel (VV) appeared to be 18 cm thick shield block comprising TiH_2, with $ZrH_{1.6}$ placed outside the BSS.

To complement the above-mentioned study, an additional set of configurations was proposed, developed and analyzed for the last DEMO HCPB design (as described here), together with assessment scheme flow paths.

The backplate at the BSS in the model was 150 mm thick. It was split to have a 50 mm EUROFER plate facing the VV and 100 mm of shielding material side by side (Figure 1). The shielding performance was analyzed at the inner shell of the VV at the equatorial IB region (the most exposed one) for the following materials selected as shielding: B_4C, WC and $YH_{1.6}$.

The shielding efficiency in terms of damage response as dpa per FPY at the VV were assessed for the baseline model and the 3 improved configurations. The dpa/FPY was computed both as cell values (Table 1) and radial profiles (Figure 2). Tabulated values are given in Table 1 at two cells around plane z = 0: one for the inner shell and one for the outer shell of the VV. Considering the inner shell of the VV, the best dpa/FPY results were obtained with an $YH_{1.6}$ shielding block used in the BSS. After ~6 cm, the behavior changed, especially for the shielding option of BSS with a WC shielding block (brown curve). This result was demonstrated to represent the best option in the rest of the VV radial depth up to the limit of the outer shell. It should be remembered at this point that the central zone of the VV comprises water and steel in a proportion of 40:60, respectively, while the two external shells comprise austenitic steel.

Table 1. Damage function (dpa/FPY) in different cells of the inner and outer VV shell at the equatorial IB level for the baseline model and 3 configurations of the BSS shielding materials.

Shielding Configuration	VV Inner Shell	VV Outer Shell
Baseline	0.1302	4.0611×10^{-5}
B_4C	0.0319	2.8009×10^{-5}
$YH_{1.6}$	**0.0290**	3.8602×10^{-5}
WC	0.0338	$\mathbf{2.0670 \times 10^{-5}}$

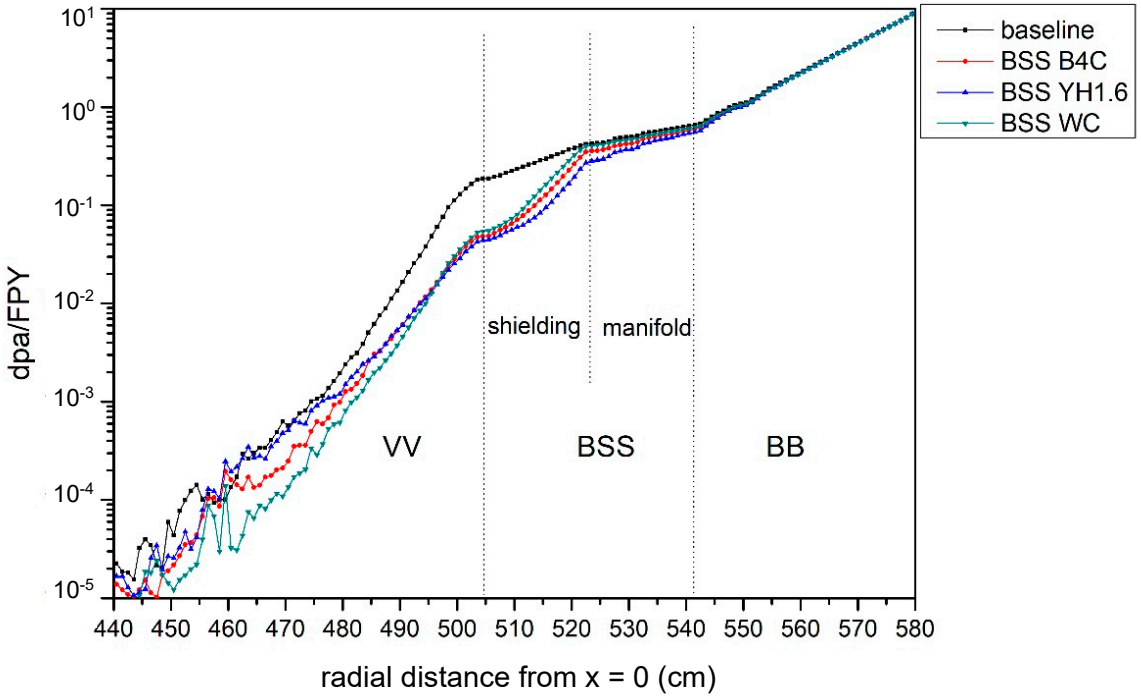

Figure 2. Radial profile at the IB equatorial plane from the FW to the VV of the dpa/FPY for the baseline model and the 3 shielding configurations.

Nuclear heating was also analyzed for the baseline case in comparison to the 3 shielding options (Figure 3). From Figure 3a, it is possible to note that all the shielding options produced significant improvement of the NH in the VV in comparison to the baseline configuration. Inside the two austenitic steel layers of 6 cm, different behavior with respect the central VV zone comprising a mixture of water and steel could be observed. In particular, in the first 6 cm of the VV, the baseline model and the models with BSS of B_4C and WC presented an ascendant behavior in the radial direction while the configuration with $YH_{1.6}$ presented a decreasing behavior (and started from values similar to the baseline case). Lower values in the first 6 cm (inner VV shell) were obtained with the BSS shielded with B_4C. The curves grew closer and closer one to each other with increasing radial depth. Again, the option of BSS with a WC shielding block (brown curve) led to changes, especially in the radial depth, and crossed the other lines. Finally, the lower values in the last 6 cm (outer VV shell) were obtained with the BSS shielded with B_4C.

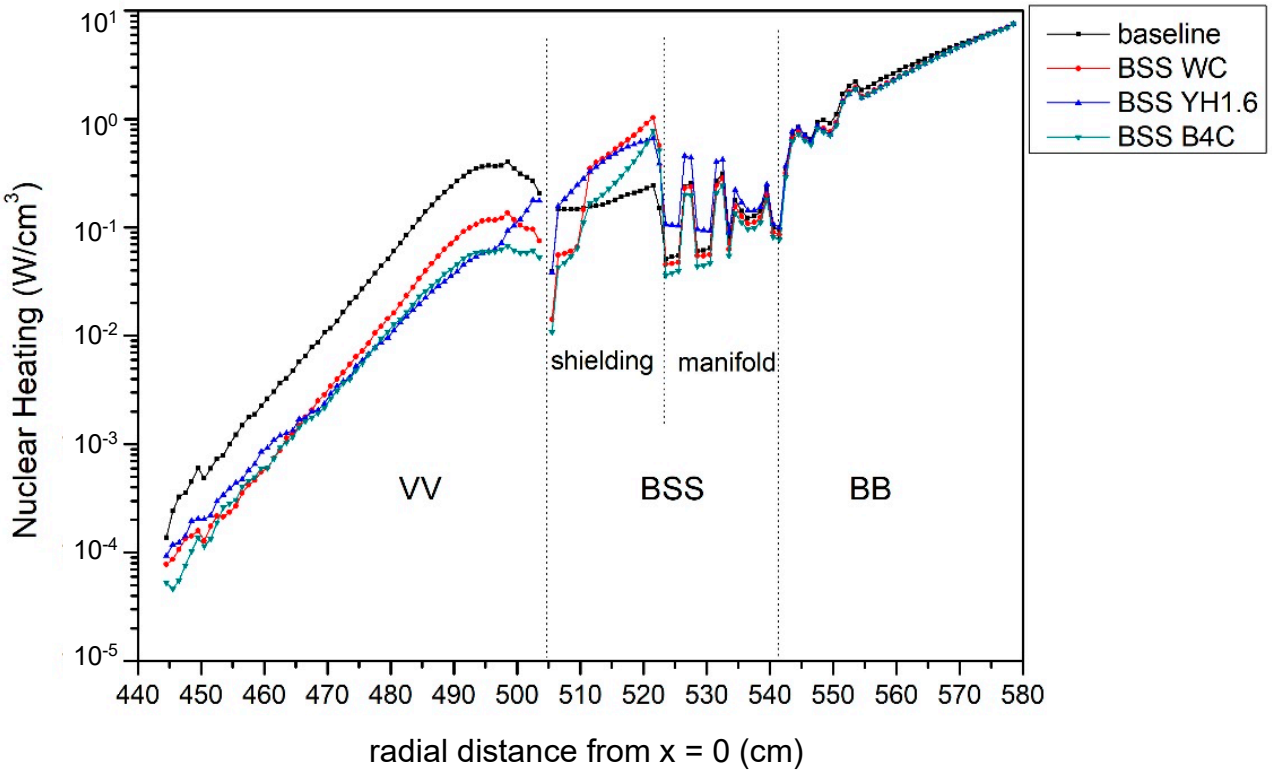

(**a**)

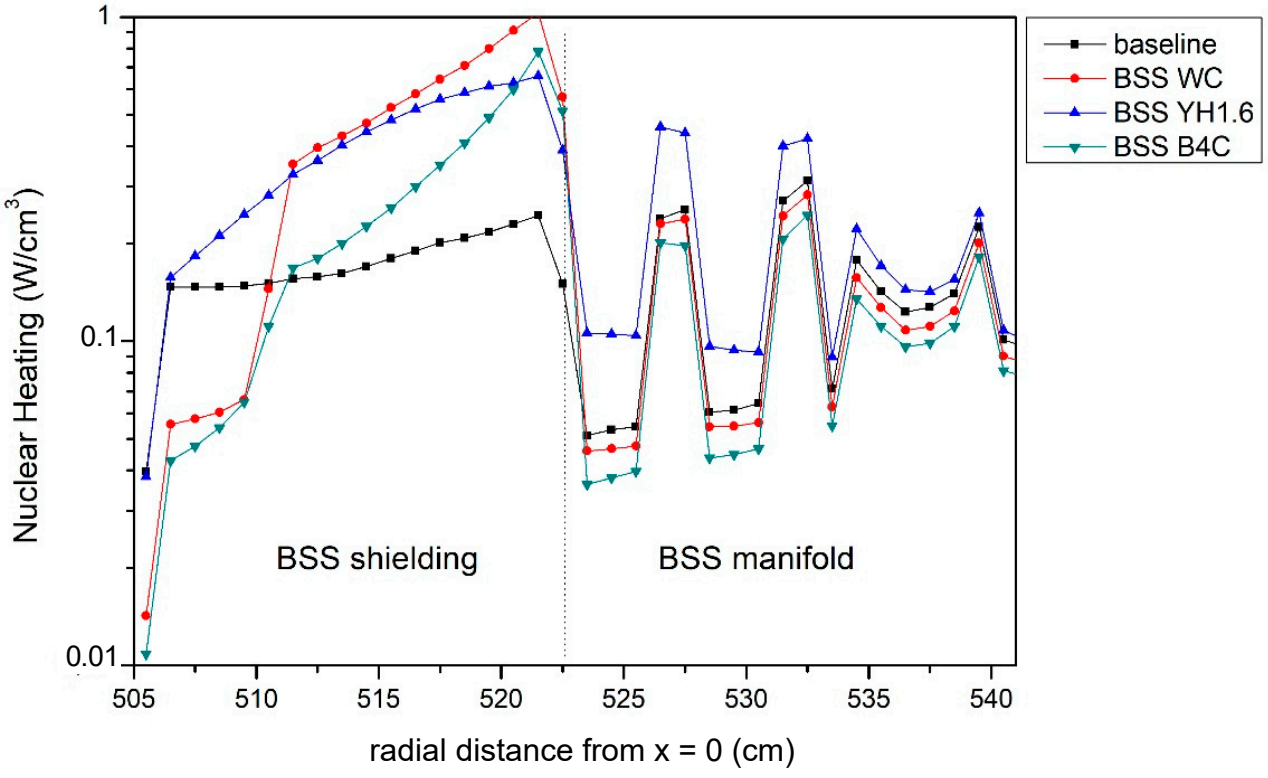

(**b**)

Figure 3. Nuclear heating radial profile at the IB equatorial plane from the FW to the VV (**a**) and just for the BSS (**b**) for the baseline model and the 3 shielding proposals.

From Figure 3b, in which just the BSS results are displayed, it is possible to observe that the baseline model and the model with the BSS shielded with 10 cm of $YH_{1.6}$ had regular, smooth decreases in the NH values over the whole 15 cm, from the 10 cm of the BSS shielding to the outer 5 cm of the Eurofer layer. On the other hand, in the curves obtained with the BSS using 10 cm of B_4C or WC, a big gap between the 10 cm shielding and the 5 cm of Eurofer can be observed. This last zone presented much more reduced values. Furthermore, the baseline model and the models with BSS of B_4C and WC produced the lowest results in the BB zone and the manifold region, indicating that they generated less backscattering in the front regions.

Due to the significant advantages in terms of safety, thermal stability (no concerns regarding hydrogen loss or tritium retention), light weight, and cost-effective fabrication of the segments of B_4C against hydrides, as well as the non-significant advantage in the shielding performance of $YH_{1.6}$ in front of B_4C, B_4C was chosen as reference for an enhanced shield. Moreover, the ITER diagnostic lines were planned to be shielded with B_4C blocks in a similar fashion as proposed in [17], which set an important practical precedent.

4. Parametric Study for B_4C BSS Shielding

A parametric study was performed by implementing different thicknesses of a B_4C external shield located in the BSS and reporting information of its effect on:

- The shielding performance in terms of nuclear heating, neutron flux and dpa in the TFC.
- Structural requirements such as nuclear heating, He production and dpa inside the VV.
- He production inside the B_4C shield (causing swelling).
- The T breeding performance (as TBR and local tritium production in the breeder and B_4C).

Ten configurations were preliminary developed and tested considering from 1 to 10 cm of B_4C thickness recovered at the expense of the Eurofer BSS thickness (of approximately 15 cm) reduced from 14 to 5 cm, respectively.

The configurations are named as follows:

- Baseline: 15 cm Eurofer (Figure 4a) and no B_4C.
- v1: 1 cm B_4C and 14 cm Eurofer (Figure 4b).
- v2: 2 cm B_4C and 13 cm Eurofer.
- v3: 3 cm B_4C and 12 cm Eurofer.
- ...
- v10: 10 cm B_4C and 5 cm Eurofer (Figure 4c).

Furthermore, another 2 configurations were implemented by inverting the position of Eurofer and B_4C for versions v5 and v10 in which, respectively, 5 cm and 10 cm of B_4C were located behind the Eurofer BSS plate. The configurations are named as follows:

- v5_inverted: 10 cm Eurofer and 5 cm B_4C.
- v10_inverted: 5 cm Eurofer and 10 cm B_4C.

The requirements followed for shielding and tritium breeding were those defined in [18–21]. For a comparison of the He production and B-10 burnup, the work of [22] was used as a reference. For the neutronic analyses, the recommendations described in the neutronic guidelines [23] were applied.

4.1. Neutronic Assessment of the Shielding Parameters

The shielding efficiency was assessed for the baseline model and the 12 improved configurations described above.

Radial profiles of nuclear heating, neutron flux, dpa and He production were produced from the FW to the TFC, also providing specific plots by "zooming" in different relevant zones. The bins in the X direction had different sizes (it is 1 cm from the FW to the first 3 cm of the VV, and 5 cm from the rest of the VV to the TFC).

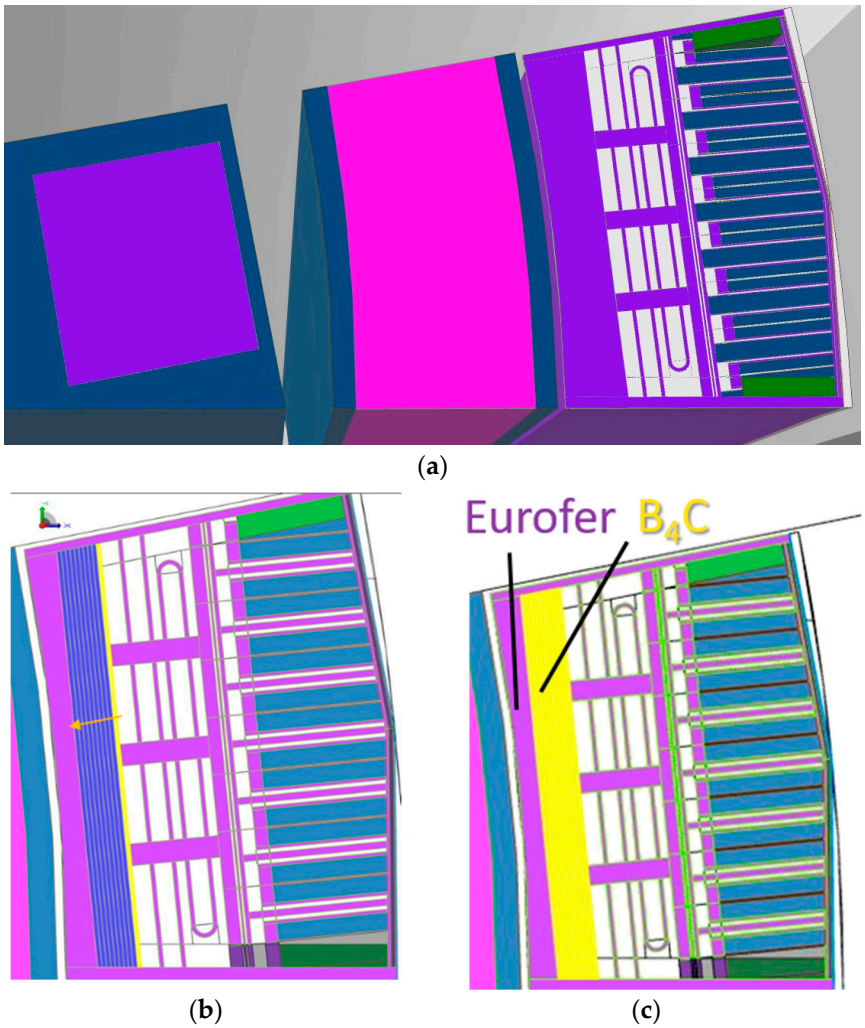

(**a**) (**b**) (**c**)

Figure 4. (**a**) HCPB baseline configuration with 15 cm Eurofer BSS (violet); (**b**) configuration v1 with 1 cm of B_4C (yellow) and 14 cm of Eurofer, with the arrow showing the direction of increasing B_4C shielding thickness from 1 cm (v1) to 10 cm of B_4C (v10); (**c**) configuration v10 with 10 cm B_4C (yellow) and approximately 5 cm of Eurofer (violet).

4.1.1. Nuclear Heating

The results of nuclear heating from the BSS to the TFC are given in Figure 5a, and in a zoomed view from the BSS to the VV in Figure 5b.

It is possible to observe that the values were generally higher in the B_4C layers of the BSS, so a high plateau, enlarged radially from v1 to v10, can be observed in that region. On the contrary, the values inside the rest of the Eurofer layers dropped, reductions that were much more evident as the space occupied by the B_4C increased.

In the rest of the components (VV and TFC), this behavior was maintained, and the values decreased from v1 to v10. Tabulated values at X = 427.5 cm (occupying the first 5 cm of the TFC Winding Pack, WP) are given for comparison in Table 2, in which the limit of 5×10^{-5} W/cm^3 inside the WP can be observed (bold values) since version 5.

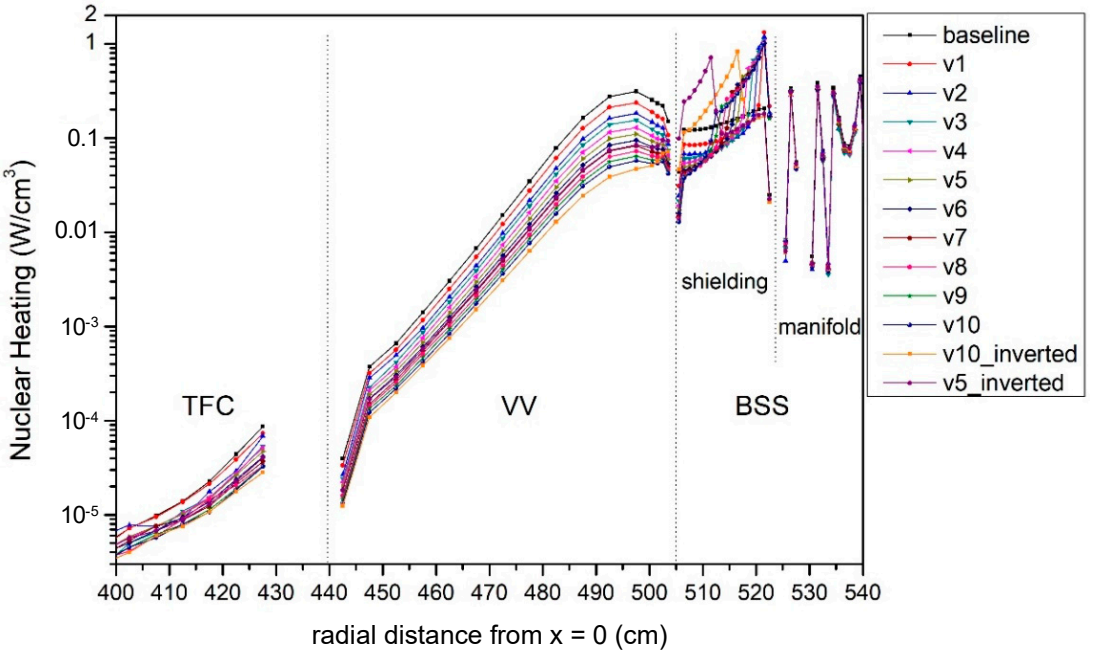

(**a**)

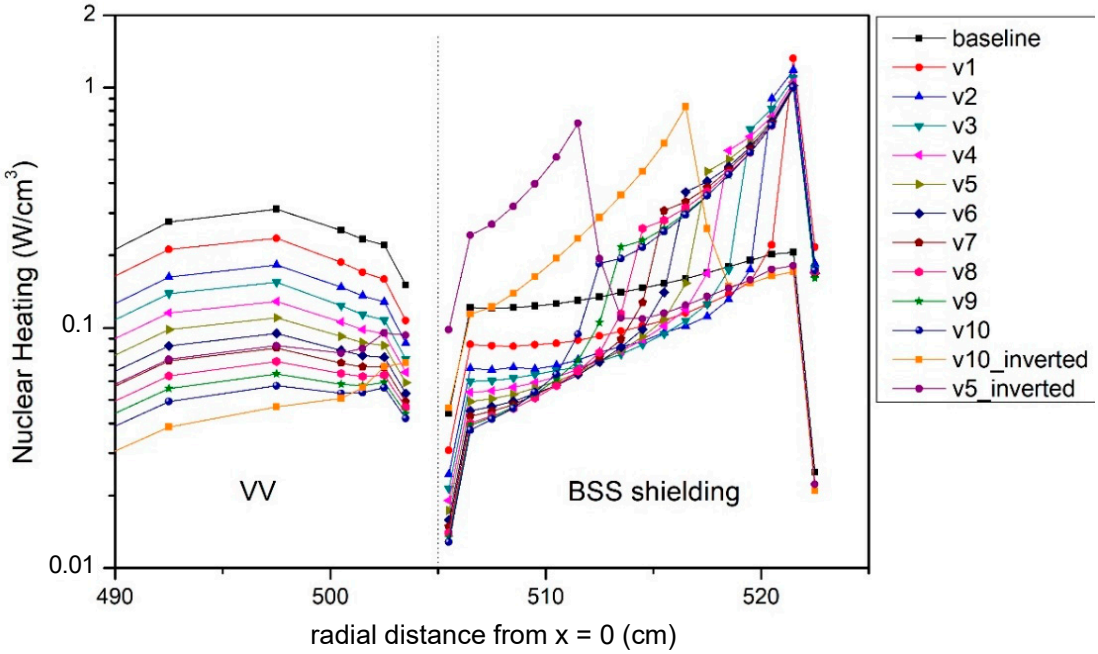

(**b**)

Figure 5. Nuclear heating for the baseline version, the 10 modified versions, and the inverted versions v5 and v10 from the BSS to the TFC (**a**); zoomed view from the BSS to the VV (**b**).

Regarding the inverted configurations, the values inside the TFC were higher for versions v10 and v5 than for the corresponding inverted versions v10_inverted and v5_inverted, respectively. The lowest values were obtained with the v10_inverted configuration: 2.81×10^{-5} W/cm^3 at the first centimeters of TFC (Table 2).

The plateau inside the BSS B4C shield is switched in position as the B_4C shield was also moved. The values in the first cms of the VV are instead higher for version inverted.

Table 2. Nuclear heating (W/cm^3) at first cm of TFC.

Analyzed Versions	X = 425–430 cm; Y = 10–15 cm; Z = 0–50 cm
baseline	8.69×10^{-5}
v1	7.36×10^{-5}
v2	6.83×10^{-5}
v3	5.37×10^{-5}
v4	5.16×10^{-5}
v5	$\mathbf{4.72 \times 10^{-5}}$
v6	$\mathbf{4.16 \times 10^{-5}}$
v7	$\mathbf{3.69 \times 10^{-5}}$
v8	$\mathbf{3.32 \times 10^{-5}}$
v9	$\mathbf{3.30 \times 10^{-5}}$
v10	$\mathbf{3.24 \times 10^{-5}}$
v5_inverted	$\mathbf{4.06 \times 10^{-5}}$
v10_inverted	$\mathbf{2.81 \times 10^{-5}}$

4.1.2. Neutron Flux

The results of neutron flux are given in Figure 6a from the BSS to the TFC, showing a zoomed view from the BSS to the VV in Figure 6b. Again, the values progressively decreased from v1 to v10 in all radial profiles.

The TFC quench limits are 1×10^{18} n/cm^2 at 6 FPY (also equivalent to 5.3×10^9 n/cm^2/s) in the epoxy and superconductor and 2×10^{17} n/cm^2 at 6 FPY (also equivalent to 1×10^9 n/cm^2/s) for the copper stabilizer. According to the tabulated results provided in Table 3, adequate shielding was provided for all versions, including the baseline model, for the epoxy and superconductor; however, these results must be confirmed for the copper stabilizer.

Table 3. Neutron flux (n/cm^2/s) at first 5 cm of TFC for the baseline model, versions v1–v10, and v5_inverted and v10_inverted.

Analyzed Versions	X = 425–430 cm; Y = 10–15 cm; Z = 0–50 cm
baseline	2.21×10^9
v1	2.07×10^9
v2	2.29×10^9
v3	1.82×10^9
v4	1.74×10^9
v5	1.66×10^9
v6	1.57×10^9
v7	1.47×10^9
v8	1.43×10^9
v9	1.41×10^9
v10	1.40×10^9
v5_inverted	1.65×10^9
v10_inverted	1.33×10^9

The ideal would be to have a detailed design for the TFC with all structures separately described rather than a homogenized composition.

Regarding the inverted configurations, the values inside the VV and TFC were higher for versions v10 and v5 than for the corresponding inverted ones, v10_inverted and v5_inverted, respectively.

The lowest values were obtained with the v10_inverted configuration. In the first centimeters of the TFC, the value was 1.33×10^9 n/cm^2/s, a little bit higher than the coil quench limit for the copper stabilizer (1×10^9 n/cm^2/s).

The tendency inside the BSS was quite different between the B_4C shield in the original and switched positions.

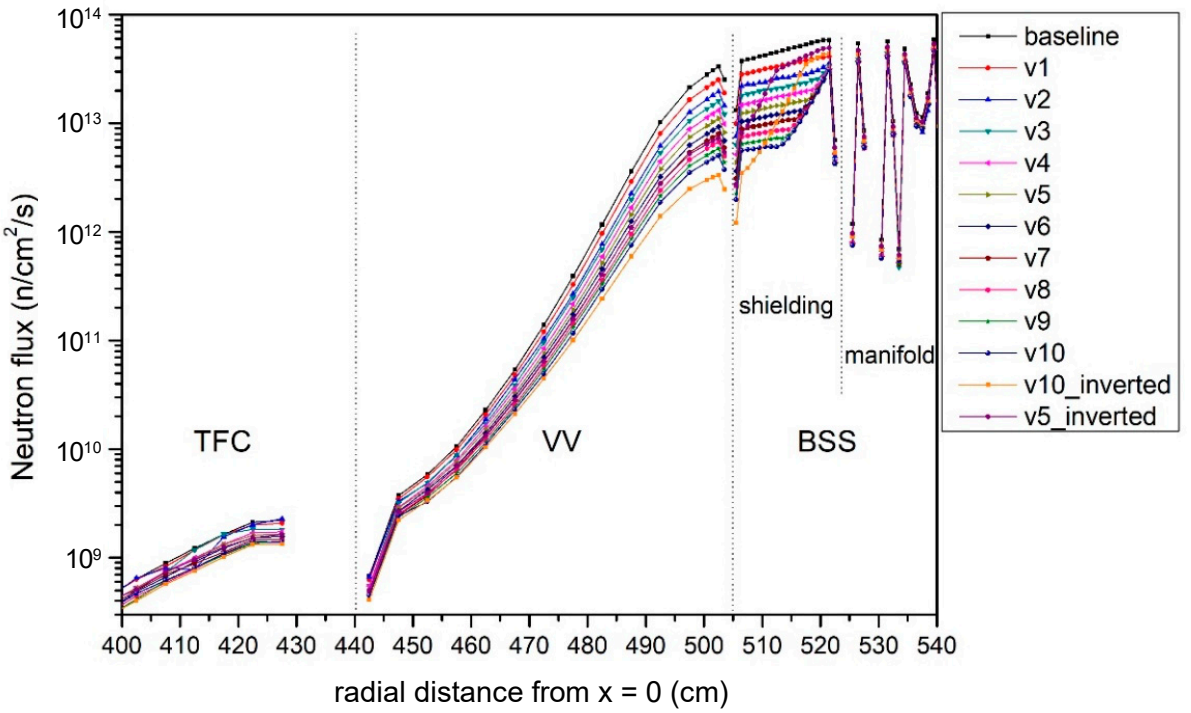

(**a**)

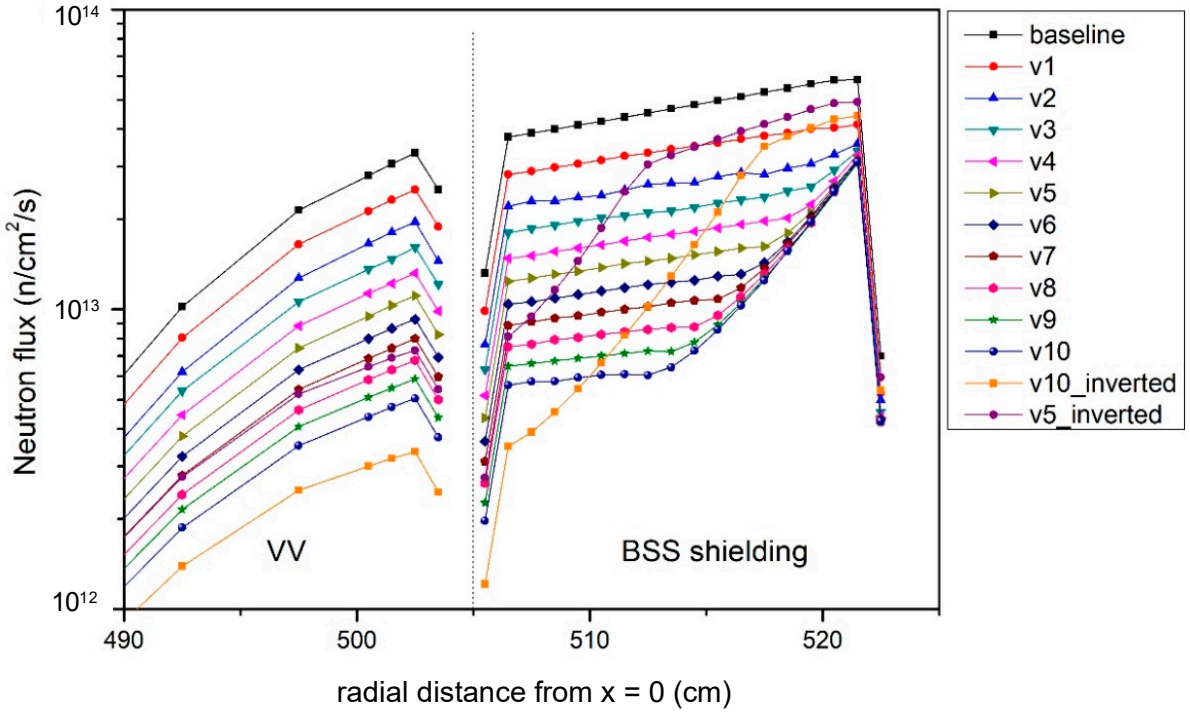

(**b**)

Figure 6. Neutron flux for the baseline model, the 10 modified versions, and inverted versions v5 and v10 from the BSS to the TFC (**a**); zoomed view from the BSS to the VV (**b**).

4.1.3. Displacement per Atom

The dpa results are given in Table 4, since the profiles were very regular. Again, the values progressively decreased from v1 to v10 in all radial profiles from the FW to the TFC.

Table 4. Damage function (dpa/FPY) at first 5 cm of TFC and at the first cm of the VV for the baseline model, versions v1–v10, and v5_inverted and v10_inverted.

Analyzed Versions	X = 425–430 cm; Y = 0–5 cm at First cm of TFC	X = 503–504 cm at First cm of VV
baseline	1.81×10^{-5}	**1.53×10^{-1}**
v1	1.69×10^{-5}	**1.28×10^{-1}**
v2	**1.24×10^{-5}**	**9.27×10^{-2}**
v3	**1.42×10^{-5}**	**9.43×10^{-2}**
v4	**1.50×10^{-5}**	**8.58×10^{-2}**
v5	**1.40×10^{-5}**	**7.70×10^{-2}**
v6	**1.41×10^{-5}**	**6.94×10^{-2}**
v7	**1.41×10^{-5}**	**6.29×10^{-2}**
v8	**1.24×10^{-5}**	**5.76×10^{-2}**
v9	**1.27×10^{-5}**	**5.52×10^{-2}**
v10	**1.24×10^{-5}**	**5.27×10^{-2}**
v5_inverted	**1.28×10^{-5}**	**7.46×10^{-2}**
v10_inverted	**1.16×10^{-5}**	**5.07×10^{-2}**

The TFC quench limit is 1×10^{-4} dpa accumulated during the 6 FPY period, equivalent to 1.6×10^{-5} dpa annual limit (dpa/FPY). According to the values of Table 4 taken in the first 5 cm of the TFC, the quench limit was fulfilled (bold) since version v2. As the recommendations were not strict and a margin was given for the dpa in the TFC ($0.5–1 \times 10^{-4}$ dpa), if the lower limit was assumed (also equivalent to 8.3×10^{-6} dpa/FPY annual limit), it was not met in any of the configurations.

The VV structural limit is 2.75 dpa accumulated during the 6 FPY period, equivalent to 0.45 dpa annual limit (dpa/FPY). According to the values of Table 4 taken in the first radial cm of the VV, the dpa limit inside the VV was confirmed to be respected (bold) since the baseline configuration.

Regarding the inverted configurations, the values inside the VV and TFC were higher for versions v10 and v5 than for the corresponding inverted ones. The lowest values were obtained with the v10_inverted configuration. At the first centimeters of the TFC, this configuration produced a value of 1.16×10^{-5} dpa/FPY, thus fulfilling the higher limit for coil quench (1.6×10^{-5} dpa/FPY) but not the lower limit (8.3×10^{-5} dpa/FPY). At the first radial cm of the VV, the dpa limit inside the VV (respected since the baseline configuration) was 5.07×10^{-2} dpa/FPY in the lowest value found for configuration v10_inverted.

4.1.4. Helium Production

The results of the helium production, as appm He/FPY radial profiles, for the baseline model and versions v1–v10 are given in Figure 7 from the BSS to the VV.

The VV structural limit is 1 appm He for the 6 FPY period, equivalent to 0.16 appm He annual limit (appm He/FPY). According to tabulated values given in Table 5, none of the versions reached this limit in the peak (column X = 490–495). The peak (see Figure 7) was located inside the VV mixture layer comprising 40% water and 60% steel. The use of a detailed VV model with steel ribs separated by water could led to different results (Section 5).

Inside the first 3 cm of the VV SS316LN layer (between approximately X = 503.5 and X = 500.5 cm, varying with the Z position from Z = 0 to Z = 50 cm), some of the versions (v9, v10, and v10_inverted) provided enough protection (bold values) to the VV steel.

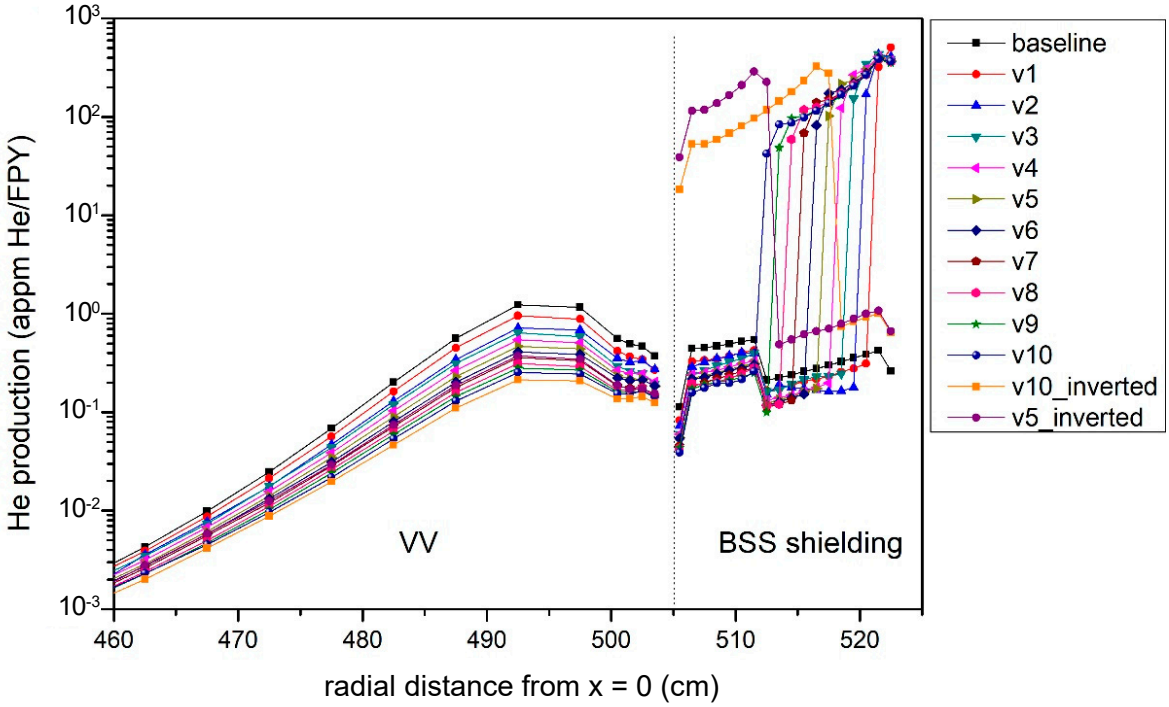

Figure 7. Helium production for the baseline model, the 10 modified versions, and inverted versions v5 and v10 from the BSS to the VV.

With the inverted configurations, the values inside the VV were lower than with the corresponding original ones. The lowest values were obtained with the v10_inverted configuration. At the first centimeters of the VV, this configuration produced a value of 0.14 appm He/FPY—lower than the 0.16 appm He/FPY VV structural limit. The high plateau inside the BSS B_4C shield was switched in position as the B_4C shield was moved. In Section 4.2, we provide analyses of the He produced in this component since the huge amount of He produced in B compound could lead to important swelling problems.

Table 5. Helium production (appm He/FPY) at the first 3 cm of the VV steel layer and inside the water and steel layer in which the peak was located for the baseline model, versions v1–v10, and v5_inverted and v10_inverted.

Analyzed Versions	Inside Water and Steel Mixed Layer		Inside ~3 cm Steel Layer			
	X = 490–495 cm	X = 495–500	X = 500–501	X = 501–502	X = 502–503	X = 503–504
baseline	1.23	1.16	0.56	0.49	0.47	0.37
v1	0.96	0.88	0.42	0.37	0.34	0.27
v2	0.72	0.68	0.35	0.32	0.33	0.27
v3	0.64	0.59	0.29	0.26	0.25	0.19
v4	0.55	0.51	0.27	0.25	0.25	0.20
v5	0.47	0.44	0.24	0.22	0.22	0.18
v6	0.41	0.39	0.22	0.21	0.21	0.19
v7	0.36	0.33	0.18	0.18	0.18	**0.15**
v8	0.31	0.29	0.17	0.17	0.18	**0.15**
v9	0.28	0.27	**0.16**	**0.16**	**0.16**	**0.14**
v10	0.25	0.25	**0.15**	**0.15**	**0.16**	**0.15**
v5_inv	0.37	0.35	0.19	0.17	0.17	**0.15**
v10_inv	0.21	0.21	**0.14**	**0.14**	**0.14**	**0.13**

4.2. Neutronic Assessment of the He and T Isotopes Global Production

The helium production inside the B_4C shield of the BSS was computed since it is directly related to the ^{10}B burnup (^{10}B transmutes in ^{7}Li via He production according to the $^{10}B(n,\alpha)^{7}Li$ reaction), with evident consequences on material degradation (such as thermal conductivity degradation and swelling)

As there is not a standard magnitude nor a limit (e.g., volumetric and annual) for He in B_4C, there were certain doubts on how to provide a representative global quantity of helium production in B_4C. For a comparison, the following paper was used as reference: [22].

For a full comparison with other possible references, the values are given in different magnitudes (Table 6): at. He per neutron source, at. He per neutron source per cm^3, appm He/FPY, and capture per m^3 (which is at. He/m^3 integrated over the time; in our case, in 6 FPY). It has to be emphasized that, when unit of capture/m^3 is used to compare the He produced during the 6 FPY of DEMO with the results of other studies, it is important to know the time other machines work. The results of at. He per neutron source and as appm He/FPY are also depicted in Figure 8a,c, respectively. As expected, the total He amount increased with the increases in B_4C thickness, but the specific values normalized to the volume were progressively lowered from v1 to v10, since a self-shielding effect allowed for fewer neutrons to react with ^{10}B.

The tritium production was computed as at. T/n for all versions v1–v10 in comparison to the baseline model (Table 7) to record the effect of the B_4C shield on the T breeding performance. The results are broken down by material (see the list of materials with the nomenclature in Table 7), including the contribution of T produced inside the B_4C shield layers.

From the baseline to version v10, a reductions in the TBR of 0.26% was found (from a TBR = 1.1734 to 1.1705), which was marginal. Furthermore, the requirement of TBR > 1.15 was still achieved.

The results of at. T per neutron source and global TBR are depicted in Figure 8b,d, respectively. As expected, the total T amount inside the B_4C increased with the increases in B_4C thickness. The TBR was progressively reduced from the baseline to v10 (as previously observed) but did not compromise the self-sufficiency of the blanket. If the T produced inside the B_4C could be also recovered, the surplus of T produced would maintain the total TBR constant at 1.1705 from v6 to v10. This means that the reduction in TBR due to the shielding (neutrons are not available to react with ^{6}Li since they are absorbed in ^{10}B) was compensated for by the increase in the local T produced inside the shield itself.

Regarding the inverted versions, the total He and T amounts inside the B_4C layer were higher for v5 and v10 than for the corresponding inverted versions. On the contrary, the total T produced inside the BB and B_4C (TBR) for versions v5_inverted and v10_inverted was higher than the corresponding original versions v5 and v10, since the new position of the B_4C shielding behind the Eurofer BSS allowed for more neutrons in the breeding structures available to produce T. The result of v5_inverted (1.172) was higher than that of v1, and the result with v10_inverted (1.1715) was higher than of v3, implying a small reduction from the baseline TBR (0.16%). Hence, the use of 10 cm B_4C in this position is viable from the point of view of T self-sufficiency.

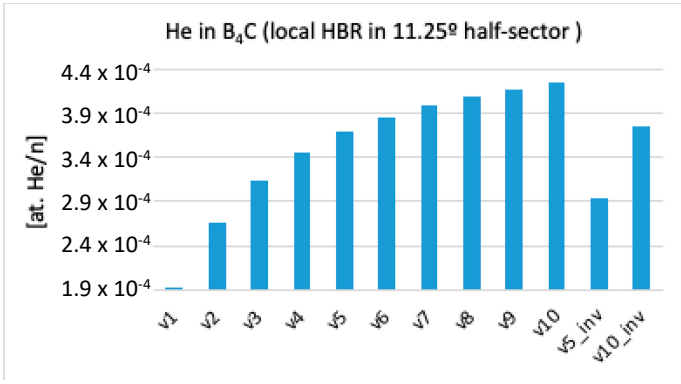

(**a**)

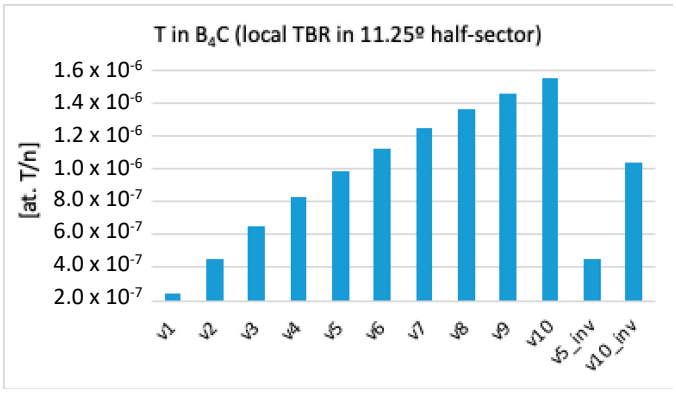

(**b**)

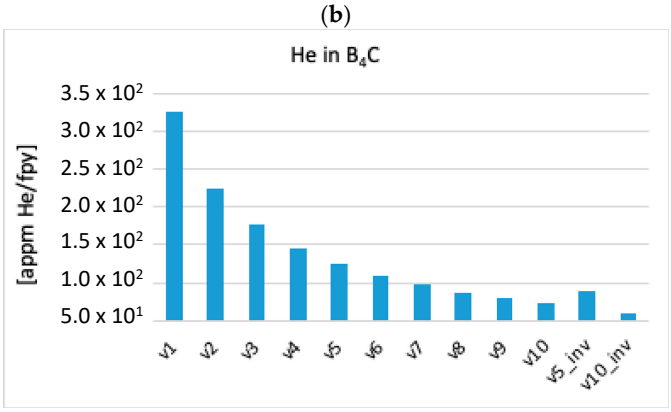

(**c**)

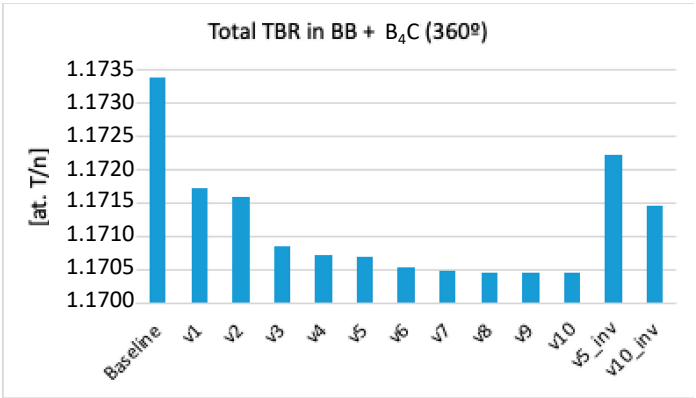

(**d**)

Figure 8. He and T production for the baseline model, the 10 modified versions, and inverted versions v5 and v10 as at. He/n (**a**), at. T/n (**b**), appm He/FPY (**c**) and total TBR (**d**).

Table 6. Helium production in different magnitudes at B_4C shield for the baseline model, versions v1–v10, and v5_inverted and v10_inverted configurations.

He in B_4C	v1	v2	v3	v4	v5	v6	v7	v8	v9	v10	v5_inv	v10_inv
HeBR at. He/n (1)	1.93×10^{-4}	2.66×10^{-4}	3.13×10^{-4}	3.45×10^{-4}	3.68×10^{-4}	3.85×10^{-4}	3.99×10^{-4}	4.09×10^{-4}	4.17×10^{-4}	4.24×10^{-4}	2.93×10^{-4}	3.74×10^{-4}
at He/cm^3 n	2.00×10^{-9}	1.38×10^{-9}	1.09×10^{-9}	8.98×10^{-10}	7.68×10^{-10}	6.70×10^{-10}	5.95×10^{-10}	5.34×10^{-10}	4.85×10^{-10}	4.44×10^{-10}	5.48×10^{-10}	3.71×10^{-10}
appmHe/fpy	325.31	224.59	176.81	146.28	125.10	109.11	96.91	87.07	79.01	72.40	89.37	60.44
cap/m^3	2.68×10^{26}	1.85×10^{26}	1.46×10^{26}	1.21×10^{26}	1.03×10^{26}	8.99×10^{25}	7.98×10^{25}	7.17×10^{25}	6.51×10^{25}	5.96×10^{25}	7.36×10^{25}	4.98×10^{25}
mol He/fpy (1)	7.18	9.87	11.64	12.82	13.69	14.31	14.81	15.19	15.49	15.76	10.88	13.90
mol He/fpy (2)	229.75	315.98	372.41	410.22	438.00	457.87	473.98	486.16	495.81	504.32	348.17	444.85

(1) in 11.25° IB vertical zone (2) in 360° IB vertical zone.

Table 7. Tritium production at the B_4C shield and the rest of the BB structures for the baseline model, versions v1–v10, and v5_inverted and v10_inverted configurations. The material numbering used in the MCNP input is maintained in this table.

(at. T/n)	Baseline	v1	v2	v3	v4	v5	v6	v7	v8	v9	v10	v5_inv	v10_inv
T in B_4C	0	2.43×10^{-7}	4.54×10^{-7}	6.55×10^{-7}	8.30×10^{-7}	9.87×10^{-7}	1.13×10^{-6}	1.25×10^{-6}	1.36×10^{-6}	1.46×10^{-6}	1.55×10^{-6}	4.53×10^{-7}	1.03×10^{-6}
T in m10	3.32×10^{-2}	3.31×10^{-2}	3.32×10^{-2}	3.31×10^{-2}	3.31×10^{-2}	3.31×10^{-2}	3.31×10^{-2}	3.31×10^{-2}	3.31×10^{-2}	3.31×10^{-2}	3.31×10^{-2}	3.32×10^{-2}	3.31×10^{-2}
T in m35	2.11×10^{-3}	2.11×10^{-3}	2.10×10^{-3}	2.11×10^{-3}	2.11×10^{-3}	2.11×10^{-3}	2.11×10^{-3}	2.11×10^{-3}	2.11×10^{-3}	2.11×10^{-3}	2.11×10^{-3}	2.11×10^{-3}	2.11×10^{-3}
T in m36	1.07×10^{-3}	1.06×10^{-3}	1.06×10^{-3}	1.06×10^{-3}	1.06×10^{-3}	1.06×10^{-3}	1.06×10^{-3}	1.06×10^{-3}	1.06×10^{-3}	1.06×10^{-3}	1.06×10^{-3}	1.07×10^{-3}	1.06×10^{-3}
T in m30	2.97×10^{-4}	2.97×10^{-4}	2.97×10^{-4}	2.97×10^{-4}	2.97×10^{-4}	2.97×10^{-4}	2.97×10^{-4}	2.97×10^{-4}	2.97×10^{-4}	2.97×10^{-4}	2.97×10^{-4}	2.97×10^{-4}	2.97×10^{-4}
tot m10—m30	3.67×10^{-2}	3.66×10^{-2}	3.66×10^{-2}	3.66×10^{-2}	3.66×10^{-2}	3.66×10^{-2}	3.66×10^{-2}	3.66×10^{-2}	3.66×10^{-2}	3.66×10^{-2}	3.66×10^{-2}	3.66×10^{-2}	3.66×10^{-2}
tot + B_4C	3.67×10^{-2}	3.66×10^{-2}	3.66×10^{-2}	3.66×10^{-2}	3.66×10^{-2}	3.66×10^{-2}	3.66×10^{-2}	3.66×10^{-2}	3.66×10^{-2}	3.66×10^{-2}	3.66×10^{-2}	3.66×10^{-2}	3.66×10^{-2}
TBR 360° in BB	1.1734	1.1717	1.1716	1.1708	1.1707	1.1707	1.1705	1.1704	1.1704	1.1704	1.1704	**1.1722**	**1.1714**
TBR 360° in BB+B_4C	1.1734	1.1717	1.1716	1.1709	1.1707	1.1707	1.1705	1.1705	1.1705	1.1705	1.1705	**1.1722**	**1.1715**
(mol T/FPY)	**Baseline**	**v1**	**v2**	**v3**	**v4**	**v5**	**v6**	**v7**	**v8**	**v9**	**v10**	**v5_inv**	**v10_inv**
T in B_4C	0	0.0090	0.0169	0.0243	0.0309	0.0367	0.0418	0.0464	0.0506	0.0542	0.0575	0.0168	0.0384
T in m10	1233.3	1231.6	1231.8	1230.7	1230.5	1230.5	1230.3	1230.3	1230.3	1230.2	1230.2	1232.1	1231.3
T in m35	78.32	78.23	78.08	78.23	78.23	78.25	78.23	78.23	78.23	78.23	78.23	78.28	78.27
T in m36	39.74	39.57	39.37	39.48	39.46	39.46	39.45	39.44	39.43	39.44	39.43	39.62	39.51
T in m30	11.04	11.03	11.04	11.03	11.03	11.03	11.03	11.03	11.03	11.03	11.03	11.03	11.03
tot m10—m30	1362.4	1360.5	1360.3	1359.4	1359.3	1359.2	1359.1	1359.0	1359.0	1358.9	1358.9	1361.0	1360.1
tot + B_4C	1362.4	1360.5	1360.3	1359.5	1359.3	1359.3	1359.1	1359.0	1359.0	1359.0	1359.0	1361.1	1360.2
tot BB 360°	43,597	43,535	43,529	43,502	43,496	43,496	43,490	43,487	43,487	43,486	43,486	43,553	43,524
tot BB+B_4C 360°	43,597	43,535	43,530	43,503	434,97	43,497	43,491	43,489	43,488	43,488	43,488	43,554	43,525

m10 = 65% Li_4SiO_4 and 35% Li_2TiO_3 with Li enriched at 60% in Li6; m35 = $Be_{12}Ti$—56.152%, Li_4SiO_4 and Li_2TiO_3—6.540%, Eurofer—21.966% (the rest is void); m36 = $Be_{12}Ti$—59.021%, Li_4SiO_4 and Li_2TiO_3—6.044%, Eurofer—21.640% (the rest is void); m30 = $Be_{12}Ti$.

5. VV Improvement Based on Borated Steels/Water Layered Configuration

In a second phase of the shielding design optimization for the HCPB BB DEMO, a detailed structure (Figure 9) was developed for the internal zone of the VV at the IB level following a similar structure to that partially described in [24] and keeping a proportion of 60:40 between steel and water layers, respectively.

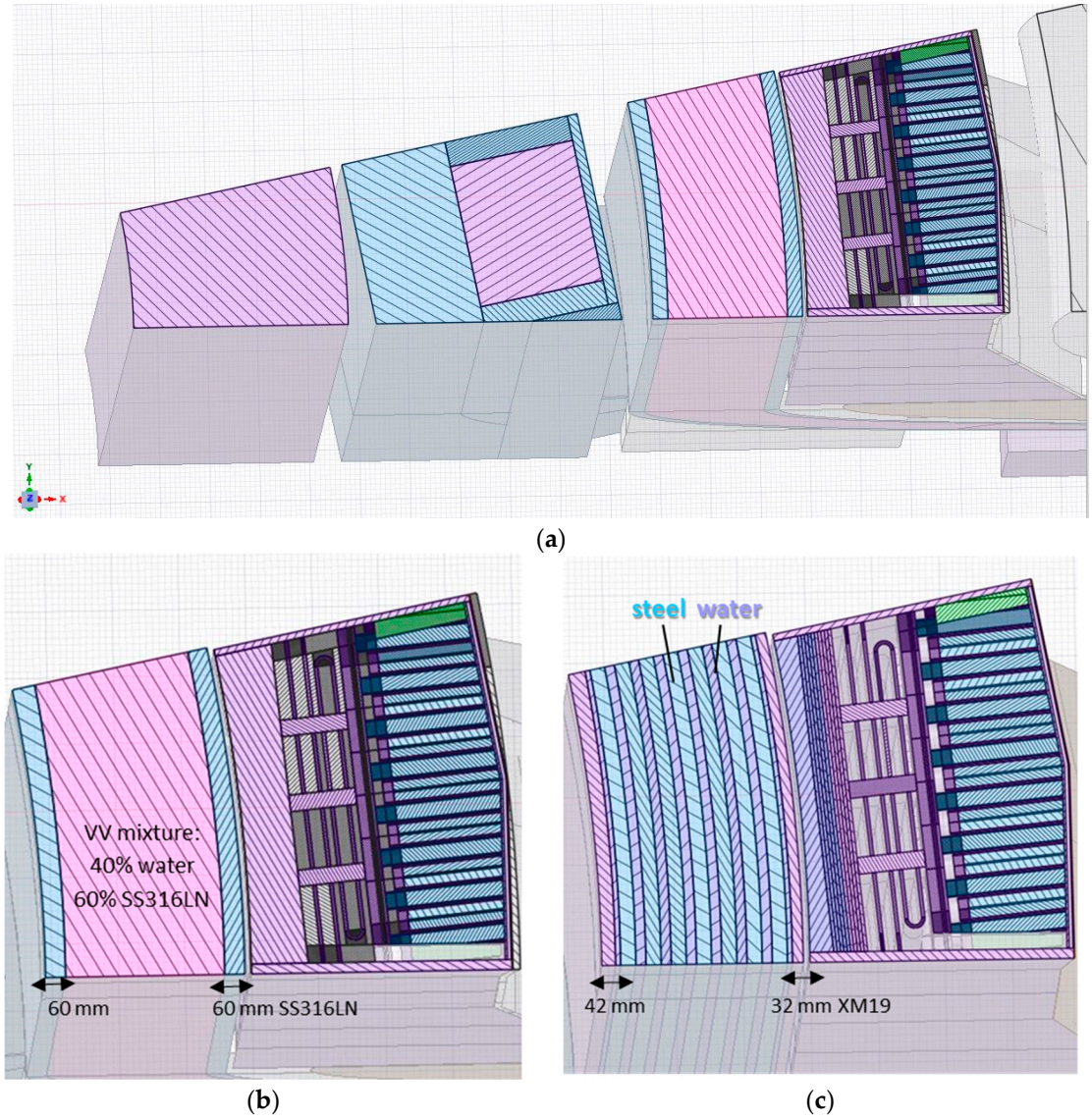

Figure 9. Horizontal section at equatorial level of the neutronic HCPB model (**a**); detail of the standard VV in the homogenized neutronic model (**b**); VV novel configuration with ribs (**c**).

In the original neutronic model (Figure 9a), the VV internal layer was represented in a simplified way by a homogenized mixture of 60% steel and 40% water (Figure 9b). A realistic configuration with internal ribs (Figure 9c) could generate different results regarding the shielding performance of the design, so it had to be addressed and perhaps enhanced.

To this end, we developed three versions of a detailed VV in which the high-strength steel XM-19 was used to strengthen the inboard wall, which allowed for reductions in the thickness of the VV shells. Thus, the 6 cm external layers of SS316LN were reduced to 3.2 cm and 4.2 cm XM-19 for the inner and outer layers, respectively. Furthermore, toroidal rather than poloidal ribs were incorporated between the two shells [24]. The specific structures of these configurations are as follows.

Configuration VV1:

- Austenitic steel XM-19 for the two external layers.
- Borated steel SS304B4 at 1.12% B for seven internal layers of 4.5 cm thickness each.
- Water at 200 °C for six filling layers of 3 cm and two border layers of 1.5 cm each.

Configuration VV2:

- Austenitic steel XM-19 for the two external layers.
- Borated steel SS304B7 at 2% B for seven internal layers of 4.5 cm thickness each.
- Water at 200 °C for 6 filling layers of 3 cm and two border layers of 1.5 cm each.

Configuration VV3:

- Austenitic steel XM-19 for the two external layers.
- Austenitic steel SS316LN for seven internal layers of 4.5 cm thickness each.
- Borated water at 1.32 wt% (0.54 vol%) and 95% ^{10}B enrichment for six filling layers of 3 cm and two border layers of 1.5 cm each.

The three configurations were tested for both the baseline-consolidated design of the HCPB and the improved BSS configuration v10_inverted previously described in Section 2.

Neutronic Assessment of the Shielding Parameters

The nuclear heating results shown in Figure 10 for the baseline and v10_inverted versions reflect the differences between the homogenized and detailed layered structures of versions VV1 and VV2 (not displayed since they were similar to VV1). For the VV3 configuration, the differences between peaks (inside the steel) and falls (inside the water) were not as pronounced as those of VV1 and VV2. The VV3 configuration produced the lowest nuclear heating values at the TFC (Table 8) in both the baseline and v10_inverted models, providing a relative reduction with the correspondent homogenized models of between 53 and 70%.

Additionally, the VV3 configuration produced the lowest values of neutron flux at the TFC (Table 9) in both the baseline and v10_inverted models. The use of the VV3 configuration brought a relative reduction with the correspondent homogenized models of between 35 and 38% at the first 5 cm of the TFC. In particular, versions v10_inverted with the VV2 and VV3 configurations fulfilled (bold values) the n flux limit of 10^9 n/cm^2/s considered for the copper stabilizer.

Furthermore, the VV3 configuration produced the lowest dpa/FPY values (Table 10) in both the baseline and v10_inverted models at the TFC level. The use of the VV3 configuration brought a relative reduction with the correspondent homogenized models of between 23 and 25% at the first 5 cm of the TFC. In particular, version v10_inverted with the VV3 configuration was nearly able to fulfil (italics) the lower dpa limit of 8.3×10^{-6} dpa/FPY (0.5 dpa at the end of life (EOF) of DEMO, which is 6 FPY) considered for the copper stabilizer.

The He production values (as appm He/FPY) shown in Figure 11 for the baseline and v10_inverted versions reflect the differences between the homogenized and detailed layered structure of versions VV1, VV2 (not displayed but similar to VV1) and VV3. Furthermore, it is possible to observe that the peaks (inside borated steel or borated water) and falls (inside normal steel or conventional water) were switched in VV3 with respect to VV1 and VV2, since the boron (which caused high He production) was inside the water and not the steel.

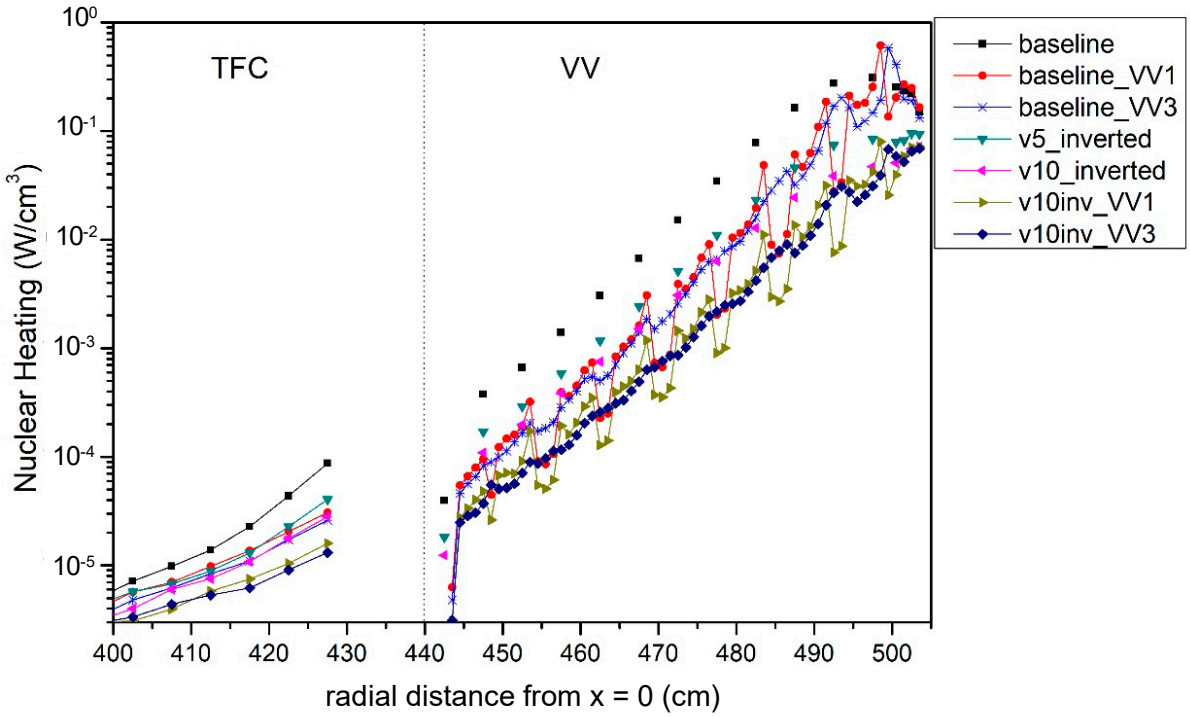

Figure 10. Nuclear heating for the baseline and v10_inverted versions with modified VV.

Table 8. Nuclear heating at first radial cm of the TFC for the baseline and v10_inverted versions with modified VV.

Nuclear Heating at First cm of TFC (X = 425–430 cm; Y = 10–15 cm; Z = 0–50 cm)			
Analyzed Versions	**W/cm^3**	**Δ% Over Baseline**	**Δ% Over v10_inverted**
Baseline	8.69×10^{-5}		
Baseline_VV1	$\mathbf{3.06 \times 10^{-5}}$	64.76%	
Baseline_VV2	$\mathbf{2.64 \times 10^{-5}}$	69.67%	
Baseline_VV3	$\mathbf{2.60 \times 10^{-5}}$	70.11%	
v10_inverted	$\mathbf{2.81 \times 10^{-5}}$	67.72%	
v10inv_VV1	$\mathbf{1.60 \times 10^{-5}}$		43.17%
v10inv_VV2	$\mathbf{1.47 \times 10^{-5}}$		47.81%
v10inv_VV3	$\mathbf{1.31 \times 10^{-5}}$		53.45%

Table 9. Neutron flux at first radial cm of the TFC for the baseline and v10_inverted versions with modified VV.

Neutron Flux at First cm of TFC (X = 425–430 cm; Y = 10–15 cm; Z = 0–50 cm)			
Analyzed Versions	**n/cm^2/s**	**Δ% Over Baseline**	**Δ% Over v10_inverted**
Baseline	2.21×10^{9}		
Baseline_VV1	1.72×10^{9}	22.46%	
Baseline_VV2	1.59×10^{9}	28.26%	
Baseline_VV3	1.36×10^{9}	38.46%	
v10_inverted	1.33×10^{9}	39.80%	
v10inv_VV1	1.07×10^{9}		20.06%
v10inv_VV2	$\mathbf{9.77 \times 10^{8}}$		26.67%
v10inv_VV3	$\mathbf{8.65 \times 10^{8}}$		35.07%

Table 10. Damage function (dpa/FPY) at first radial cm of the TFC for the baseline and v10_inverted versions with modified VV.

dpa/FPY at First cm of TFC (X = 425–430 cm; Y = 0–5 cm; Z = 0–50 cm)			
Analyzed Versions	**dpa/FPY**	**Δ% Over Baseline**	**Δ% Over v10_inverted**
Baseline	1.81×10^{-5}		
Baseline_VV1	1.57×10^{-5}	13.13%	
Baseline_VV2	1.49×10^{-5}	17.81%	
Baseline_VV3	1.34×10^{-5}	25.98%	
v10_inverted	1.16×10^{-5}	35.85%	
v10inv_VV1	9.60×10^{-6}		17.40%
v10inv_VV2	9.94×10^{-6}		14.42%
v10inv_VV3	8.94×10^{-6}		23.00%

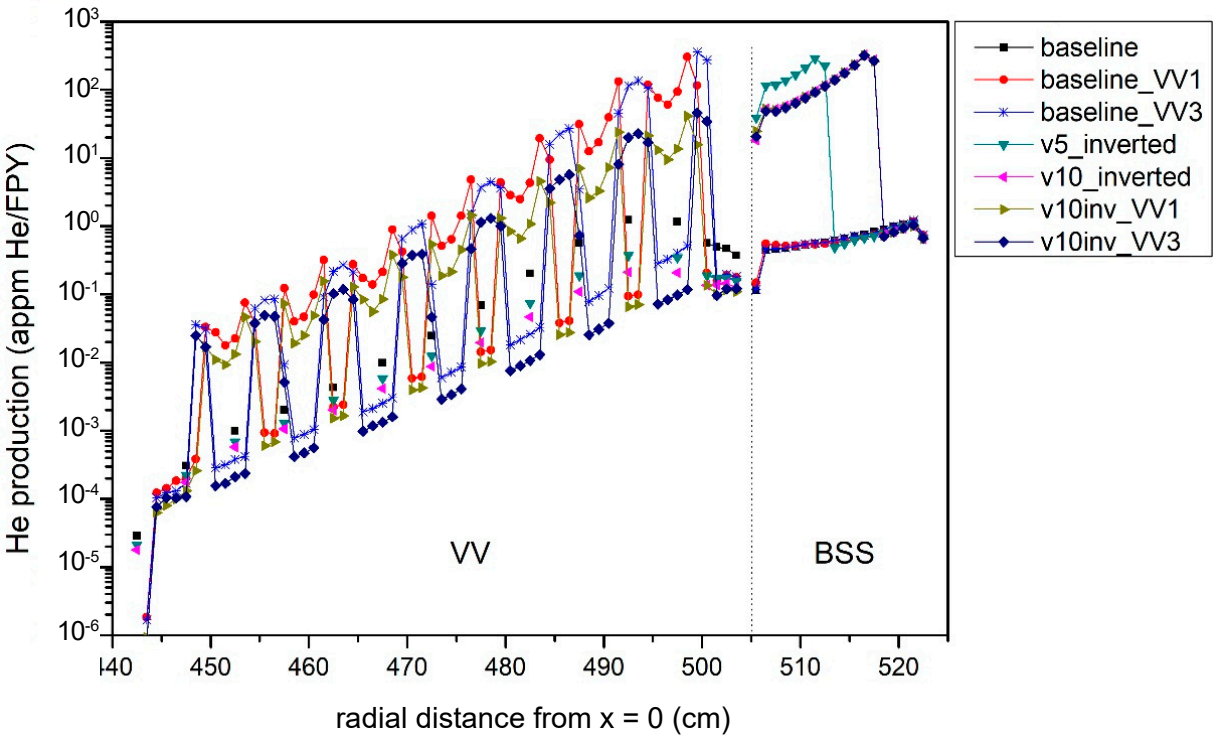

Figure 11. Helium production (appm He/FPY) as radial profile from the BSS to the TFC for the 3 VV new configurations applied to the baseline and v10_inverted versions in comparison to the standard baseline, v5_inverted and v10_inverted versions.

Accordingly, the VV3 configuration produced the lowest values inside the internal steel layers (Table 11) in both the baseline and v10_inverted models, producing significant differences from ≈300 (VV1 and VV2) to ≈0.5 (VV3) appm/FPY in the baseline cases and from ≈40 (VV1 and VV2) to ≈0.1 (VV3) appm/FPY in the v10_inverted cases. The internal steel layers of the v10_inverted_VV3 configuration could reach the 0.16 appm He/FPY limit (green values).

In the external layers, the differences between using SS316LN or XM-19 were marginal: from 0.5 to 0.2 (approximately) for the baseline case and from 0.14 to 0.11 (approximately) for the v10_inverted cases. Hence, all versions of v10_inverted with both standard and multi-layered VV structures fulfilled the 0.16 appm He/FPY limit inside the external steel layer.

Table 11. Helium production in the VV for the baseline and v10_inverted versions with modified VV.

Analyzed Versions	appm He/fpy at the VV (at Y = 5–10 cm; Z = 0–50 cm)						
	Internal Layers			Inside ~3 cm External Steel Layer [2]			
	X= 495–500 cm [1]			X = 500–501 [3]	X = 501–502	X = 502–503	X = 503–504
Baseline [1]	1.16			0.56	0.49	0.47	0.37
	X= 497–498	**X = 498–499**	**X = 499–500**	**X = 500–501**	**X = 501–502**	**X = 502–503**	**X = 503–504**
Baseline_VV1	94.54	305.96	116.00	0.206	0.161	0.191	0.178
Baseline_VV2	99.51	323.01	154.45	0.233	0.174	0.204	0.189
Baseline_VV3 [4]	0.40	0.52	359.28	274.30	0.162	0.193	0.183
	X= 495–500 cm [1]			**X = 500–501**	**X = 501–502**	**X = 502–503**	**X = 503–504**
v10_inverted [1]	0.21			0.136	0.137	0.145	0.125
	X= 497–498	**X = 498–499**	**X = 499–500**	**X = 500–501**	**X = 501–502**	**X = 502–503**	**X = 503–504**
v10inv_VV1	13.65	41.15	15.72	0.135	0.099	0.116	0.109
v10inv_VV2	13.78	41.53	19.63	0.136	0.102	0.120	0.115
v10inv_VV3 [4]	0.098	0.117	45.92	34.33	0.096	0.120	0.121

[1] For the baseline and v10_inverted configuration with a standard resolution of 5 cm inside VV, such values fell inside the water and steel VV mixture layer. [2] The external layer comprised SS316LN for baseline and v10_inverted with standard VV; XM-19 for baseline and v10_inverted with VV1, VV2, and VV3 configurations. [3] This bin of 1 cm was part of the SS316LN external layer of 6 cm for the VV standard or was a water layer for VV1, 2, and 3. As the mesh discretization did not exactly cover the layer scheme, a voxel could contain two different layers. [4] For VV3, as the boron (which led to high He production) was inside the water and not the steel, peaks and falls were switched with respect to VV1 and VV2. Again, as the mesh discretization did not exactly cover the layer scheme, a voxel could contain two different layers.

6. Discussion and Conclusions

In support of the HCPB design, neutronics studies have been focused on shielding improvements, considering solutions that could adequately protect the vacuum vessel (VV) and toroidal field coils (TFCs).

Several shielding options were previously studied in terms of architecture (e.g., in-BB shield and ex-BB shield) and materials (e.g., B_4C, WC, WB, YHx, and ZrHx). The most attractive design has been that based on B_4C blocks, which was chosen in this research as a reference for an enhanced shield and studied in depth.

In this context, the authors of the present paper present the main results for two studies:

- We performed a parametric study by implementing different thicknesses (from 1 to 10 cm) of a B_4C external shield located in the BSS behind the BZ or behind the Eurofer BSS and by reporting information of the effect on the shielding performance and helium production inside the B_4C and TBR. Furthermore, three configurations were developed elaborating a detailed structure for the internal layer of the VV at the inboard side. Three combinations of different steels and water were tested, i.e., VV1: SS304B4 at 1.12% B/water; VV2: SS304B7 at 2% B/water; and VV3: SS316LN/borated water at 1.32 wt% (0.54 vol%). Corresponding shielding analyses were conducted regarding influence on neutron attenuation when implementing such a VV structure for both the baseline consolidated HCPB design and an improved BSS configuration.

General conclusions are as follows:

- For all the shielding and structural responses, the values were progressively reduced from the baseline to v10 with the 10 cm B_4C shield.
- Furthermore, the inverted configurations with B_4C behind the Eurofer BSS and facing the VV produced lower values than the original (opposite) corresponding ones.
- The three VV structure configurations showed to values lower than those of the original homogenized VV mixture, except for the helium production in borated steels.
- Version VV3 with borated water and standard steel was found to be the best option in terms of shielding responses.

According to the results of the shielding and structural responses, it can be summarized that:

- No special concern is needed regarding the VV nuclear heating and dpa, since the structural limits of the VV were observed from the baseline configuration.
- The nuclear heating quench limit in the TFC was respected since version v5 with 5 cm B_4C.
- The most critical responses were the neutron flux and dpa. The neutron flux quench limit of 5.3×10^9 n/cm^2/s in the epoxy and superconductor was fulfilled for all the configurations, but the limit of 1×10^9 n/cm^2/s for the copper stabilizer was only fulfilled using improved VV configurations: v10inverted_VV2 and v10inverted_VV3 (or nearly to be accomplished in v10inverted_VV1); regarding the dpa in the TFC, the quench limit of 1×10^{-4} dpa was fulfilled since version v2. As recommendations are not strict and a margin is allowed for dpa in the TFC copper stabilizer ($0.5 - 1 \times 10^{-4}$ dpa), none of the configurations fulfilled the lower limit of 0.5×10^{-4} dpa, with only version v10_inverted_VV3 close to fulfilling it.
- Regarding the helium production in VV steel, it was possible to see that the limit of 1 appm was observed in v9, v10, v10_inverted, v10_inverted_VV3, and only in the external steel layers of v10_inverted_VV1 and VV2. For the internal steels layers of such VV versions VV1 and VV2, which contained boron, the values were one or two orders of magnitude higher than the limit.

According to the global isotope production responses:

- Regarding the T production inside the breeding blanket and BSS, it was possible to observe that the B_4C shield did not have a relevant impact on the T breeding performance since the loss of TBR from the baseline (TBR = 1.1734) in the worst case (10 cm of B_4C, TBR = 1.1705) was 0.26% and thus marginal. Furthermore, the requirement of TBR > 1.15 was still achieved. The impact was lower when the inverted configurations were used.
- If the T produced inside the B_4C could be recovered, the surplus of T produced there could maintain the total TBR constant at 1.1705 from v6 to v10. This means that the reduction in TBR due to the thicker shielding (neutrons not available to react with ^{6}Li since they are absorbed in ^{10}B) was compensated by the increase in the local T produced inside the shield itself.
- Furthermore, as expected, the total He amount inside the B_4C shield increased with the increase in B_4C thickness, but the specific values normalized to the volume were progressively lowered from v1 to v10 since a self-shielding effect allowed for fewer neutrons to react with ^{10}B. The total He amount inside the B_4C layer was higher for v5 and v10 than for the corresponding inverted versions.
- Similar behavior was observed for the T production inside B_4C, although the global amount was three orders of magnitude less than that of the He production, demonstrating that the retention of this radioisotope is of no special concern.

Based on the results of this paper, research regarding the detailed design of a B_4C shield with thermal and structural analyses is in progress in order to provide a complete picture of an engineering solution for a shielding enhancement of the HCPB concept.

Author Contributions: Conceptualization, I.P., F.A.H., P.P., D.R. and G.Z.; methodology, I.P. and P.P.; formal analysis, I.P.; investigation, I.P.; data curation, I.P.; writing—original draft preparation, I.P.; writing—review and editing, I.P., F.A.H. and G.Z.; visualization, I.P. and G.Z.; supervision, F.A.H., P.P., D.R. and G.Z.; project administration, F.A.H., D.R. and G.Z. All authors have read and agreed to the published version of the manuscript.

Funding: This work has been carried out within the framework of the EUROfusion Consortium, funded by the European Union via the Euratom Research and Training Programme (Grant Agreement No 101052200—EUROfusion). Views and opinions expressed are, however, those of the author(s) only and do not necessarily reflect those of the European Union or the European Commission. Neither the European Union nor the European Commission can be held responsible for them.

Acknowledgments: The authors acknowledge funding by the Community of Madrid (TechnoFusión (III)-CM (S2018/EMT-4437) project co-financing with structural funds (ERDF and ESF)). The authors would like to thank the FDS Team for providing SuperMC.

Conflicts of Interest: The authors declare no conflict of interest. The funders had no role in the design of the study; in the collection, analyses, or interpretation of data; in the writing of the manuscript, or in the decision to publish the results.

References

1. Hernández, F.A.; Pereslavtsev, P.; Zhou, G.; Kang, Q.; D'Amico, S.; Neuberger, H.; Boccaccini, L.V.; Kiss, B.; Nadasi, G.; Maqueda, L.; et al. Consolidated design of the HCPB Breeding Blanket for the pre-Conceptual Design Phase of the EU DEMO and harmonization with the ITER HCPB TBM program. *Fusion Eng. Des.* **2020**, *157*, 111614. [CrossRef]
2. Hernández, F.A.; D'Amico, S.; Neuberger, H.; Pereslavtsev, P.; Retheesh, A.; Zhou, G. Final Report on Deliverable Design and Integration Studies 2020. BB-1.2.1-T007-D001, EFDA_D_2NUZCR. 2021. Available online: https://idm.euro-fusion.org/default.aspx?uid=2NUZCR (accessed on 13 July 2022).
3. Palermo, I. Final Report on Deliverable Neutronics Support 2018 (CIEMAT); BB-1.2.1-T005-D006 EFDA_D_2NBMNT; 2020. Available online: https://idm.euro-fusion.org/default.aspx?uid=2NBMNT (accessed on 13 July 2022).
4. X-5 Monte Carlo Team. MCNP—A General Monte Carlo N-Particle Transport Code, Version 5 2003, LA-UR-03-1987. Available online: https://mcnp.lanl.gov/pdf_files/la-ur-03-1987.pdf (accessed on 13 July 2022).
5. The JEFF-3.2 Nuclear Data Library. Nuclear Energy Agency, Oecd. Available online: https://www.oecd-nea.org/dbforms/data/eva/evatapes/jeff_32/ (accessed on 1 January 2017).
6. Wu, Y.; FDS Team. CAD-based interface programs for fusion neutron transport simulation. *Fusion Eng. Des.* **2009**, *84*, 1987–1992. [CrossRef]
7. Norgett, M.J.; Robinson, M.T.; Torrens, I.M. A proposed method of calculating displacement dose rates. *Nucl. Eng. Des.* **1975**, *33*, 50–54. [CrossRef]
8. Federici, G.; Bachmann, C.; Barucca, L.; Biel, W.; Boccaccini, L.; Brown, R.; Bustreo, C.; Ciattaglia, S.; Cismondi, F.; Coleman, M.; et al. DEMO design activity in Europe: Progress and updates. *Fusion Eng. Des.* **2018**, *136*, 729–741. [CrossRef]
9. Bachmann, C.; Ciattaglia, S.; Cismondi, F.; Eade, T.; Federici, G.; Fischer, U.; Franke, T.; Gliss, C.; Hernandez, F.; Keep, J.; et al. Overview over DEMO design integration challenges and their impact on component design concepts. *Fusion Eng. Des.* **2018**, *136*, 87–95. [CrossRef]
10. Wenninger, R. DEMO1 PROCESS Full output (May 2017), EFDA_2NDSKT_v1_0. And PROCESS Two Page Output (EFDA_D_2NE9JA v1.0). Available online: https://idm.euro-fusion.org/default.aspx?uid=2NE9JA (accessed on 13 July 2022).
11. Hernández, F.A.; Pereslavtsev, P.; Zhou, G.; Neuberger, H.; Rey, J.; Kang, Q.; Boccaccini, L.V.; Bubelis, E.; Moscato, I.; Dongiovanni, D. An enhanced, near-term HCPB design as driver blanket for the EU DEMO. *Fusion Eng. Des.* **2019**, *146*, 1186–1191. [CrossRef]
12. Hernández, F.A.; Pereslavtsev, P. First principles review of options for tritium breeder and neutron multiplier materials for breeding blankets in fusion reactors. *Fusion Eng. Des.* **2018**, *137*, 243–256. [CrossRef]
13. Knitter, R.; Kolb, M.; Kaufmann, U.; Goraieb, A. Fabrication of modified lithium orthosilicate pebbles by addition of titania. *Fusion Eng. Des.* **2013**, *442*, 433–436. [CrossRef]
14. Kolb, M.H.H.; Mukai, K.; Hoshino, T. Li_4SiO_4 based breeder ceramics with Li_2TiO_3, $LiAlO_2$ and $Li_XLa_YTiO_3$ additions, part I: Fabrication. *Fusion Eng. Des.* **2017**, *115*, 39–48. [CrossRef]
15. Kolb, M.H.H.; Knitter, R.; Hoshino, T. Li_4SiO_4 based breeder ceramics with Li_2TiO_3, $LiAlO_2$ and $Li_XLa_YTiO_3$ additions, part II: Pebble properties. *Fusion Eng. Des.* **2017**, *115*, 6–16. [CrossRef]
16. Pereslavtsev, P.; Cismondi, F.; Hernández, F.A. Analyses of the shielding options for HCPB DEMO blanket. *Fusion Eng. Des.* **2020**, *156*, 111605.
17. Juárez, R.; Guirao, J.; Kolsek, A.; Lopez, A.; Pedroche, G.; Bertalot, L.; Udintsev, V.S.; Walsh, M.J.; Sauvan, P.; Sanz, J. The use of the long modular diagnostics shield module to mitigate shutdown dose rates in the ITER diagnostics equatorial ports. *Nucl. Fusion* **2018**, *58*, 056015. [CrossRef]
18. Fischer, U.; Bachmann, C.; Palermo, I.; Pereslavtsev, P.; Villari, R. Neutronics requirements for a DEMO fusion power plant. *Fusion Eng. Des.* **2015**, *98–99*, 2134–2137. [CrossRef]
19. Duchateau, J.-L.; Hertout, P.; Saoutic, B.; Magaud, P.; Artaud, J.-F.; Giruzzi, G.; Bucalossi, J.; Johner, J.; Sardain, P.; Imbeaux, F.; et al. Conceptual design for the superconducting magnet system of a pulsed DEMO reactor. *Fusion Eng. Des.* **2013**, *88*, 1609–1612. [CrossRef]
20. Harman, J. WP12 DEMO Operational Concept Description. EFDA_D_2LCY7A. 2012. Available online: https://idm.euro-fusion.org/default.aspx?uid=2LCY7A (accessed on 13 July 2022).
21. Fischer, U.; Boccaccini, L.; Cismondi, F.; Coleman, M.; Day, C.; Hörstensmeyer, Y.; Moro, F.; Pereslavtsev, P. Required, achievable and target TBR for the European DEMO. *Fusion Eng. Des.* **2020**, *155*, 111553. [CrossRef]
22. Maruyama, T.; Onose, S.; Kaito, T.; Horiuchi, H. Effect of Fast Neutron Irradiation on the Properties of Boron Carbide Pellet. *J. Nucl. Sci. Technol.* **1997**, *34*, 1006–1014. [CrossRef]

23. Fischer, U. Guidelines for Neutronic Analyses. EFDA_D_2L8TR9 v1.8. 2020. Available online: https://idm.euro-fusion.org/default.aspx?uid=2L8TR9 (accessed on 13 July 2022).
24. Bachmann, C.; Ciupinski, L.; Gliss, C.; Franke, T.; Härtl, T.; Marek, P.; Maviglia, F.; Mozzillo, R.; Pielmeier, R.; Schiller, T.; et al. Containment structures and port configurations. *Fusion Eng. Des.* **2022**, *174*, 112966. [CrossRef]